Available online at www.sciencedirect.com

ScienceDirect

Geochimica et Cosmochimica Acta xxx (2022) xxx–xxx

Geochimica et Cosmochimica Acta

www.elsevier.com/locate/gca

An experimental and thermodynamic study of sphalerite solubility in chloride-bearing fluids at 300–450 °C, 500 bar: implications for zinc transport in seafloor hydrothermal systems

Yanlu Xing [a,b,*], Joël Brugger [b], Peter Scheuermann [a,c], Chunyang Tan [a], Shichao Ji [a], William E. Seyfried Jr. [a]

[a] Department of Earth and Environmental Sciences, University of Minnesota Twin Cities, Minneapolis, MN 55455, USA
[b] School of Earth, Atmosphere and Environment, Monash University, Clayton, VIC 3800, Australia
[c] Department of Earth, Ocean and Atmospheric Sciences, University of British Columbia, Vancouver, BC V6T 1Z4, Canada

Received 26 May 2021; accepted in revised form 20 March 2022; available online xxxx

Abstract

The solubility and speciation of zinc (Zn) in chloride-bearing aqueous fluids at high temperature and pressure are important for understanding Zn transport in natural hydrothermal systems and associated mineralizing processes. Here, we measured sphalerite solubility in NaCl-HCl-H_2O fluids using a fixed-volume titanium alloy hydrothermal reactor equipped with a newly designed gas-tight titanium piston sampler. This novel reactor-sampling system is capable of acquiring internally filtered fluids at high temperature and pressure. The experiments were conducted at 300–450 °C, 500 bar, in fluid with 0.5 m and 1 m NaCl, respectively. The measured sphalerite solubilities are consistent with predicted values using previous thermodynamic data at 300–400 °C, but diverge significantly above 400 °C. To resolve this discrepancy, we adjusted the solubility product of Zn minerals by modifying the heat capacity and Born coefficients that describe the Gibbs Free Energy of formation from the elements of the Zn^{2+} aqua ion based on the new solubility data. The refined Helgeson-Kirkham-Flowers (HKF) equation of state (EoS) of Zn^{2+} empirically reproduces the solubility data of Zn minerals from previous experimental studies well over the covered T-P range (25–600 °C, P_{sat} to 2 kbar), but extends accurate predictions to conditions typical of deep sea hydrothermal systems, down to fluid densities of 0.35 g/cm^3. Thermodynamic modelling using the revised EoS of Zn^{2+} shows that higher temperatures, chlorinity and lower pH increase Zn solubility, and that Zn chloride complexes are the predominant species. The influence from salinity on Zn solubility is less significant in fluids with low pH. Applied to seafloor hydrothermal systems, our results suggest that in addition to temperature, pH and total dissolved chloride, fluid/rock ratio may be an important factor contributing to Zn concentrations in vent fluids at Mid Ocean Ridges.

Keywords: Zinc transport; Hydrothermal experiment; Thermodynamic modelling; Seafloor hydrothermal system; Fluid/rock ratio

1. INTRODUCTION

Most of the world's zinc (Zn) resources are of hydrothermal origin (Brugger et al., 2016). In seafloor hydrothermal systems, vent fluids usually have elevated Zn (up to a few hundreds of μmol/kg; Tivey, 1995; Edmonds et al., 1996; Seyfried et al., 2003; Von Damm et al., 2003; Gallant and Von Damm, 2006; Seyfried et al., 2011), contrasting sharply with the low Zn contents present in seawater (≪ 0.15 μmol/kg; Neff, 2002). As a result, sphalerite (ZnS) is widely observed in seafloor sulfide

* Corresponding author.
E-mail address: yanluxxing@gmail.com (Y. Xing).

https://doi.org/10.1016/j.gca.2022.03.026
0016-7037/

structures, i.e., 'Black Smokers' (German and Seyfried, 2014), and Zn can provide information on the fluid-rock interactions in the root zone of seafloor hydrothermal systems characterized by high pressure and temperature. However, solubility data for Zn minerals, such as sphalerite and/or zincite (ZnO), are scarce at temperatures above 350 °C, especially at pressure conditions characteristic of seafloor systems (400–600 bar), which limits our understanding of Zn transport and complexing behavior in aqueous fluids at high T-P conditions.

Solubility experiments provide direct constraints on the capacity of fluids to carry metals, but they are still beset by experimental difficulties (e.g., Crerar et al., 1985; Barnes, 1997; and references therein). In particular, sampling of high temperature solutions in a manner that accurately records *in-situ* compositions of fluid equilibrated with the buffering mineral assemblage is key to reliable measurements. In the case of Zn, solubility is highly sensitive to temperature (Hemley et al., 1992; Cygan et al., 1994; Yardley, 2005; Akinfiev and Tagirov, 2014; Mei et al., 2015; Etschmann et al., 2019). Quenching-based experiments using sealed gold/platinum capsules have been widely used for solubility experiments at high T-P conditions, i.e., 300–600 °C, 500–2000 bar (Plyasunov and Ivanov, 1990; Hemley et al., 1992; Cygan et al., 1994; Akinfiev and Tagirov, 2014). For such experiments, quenching is performed as rapidly as possible to maintain the *in-situ* fluid composition found at high temperature and pressure; however, the coexistence of minerals and fluids together in the cooling capsules introduces uncertainty in metal concentrations during quenching. To address this issue, Tagirov and Seward (2010) used a flow-through Ti-Pd alloy reactor system. Their new system greatly improves operational procedures and allows *in-situ* sampling of high T-P fluids, although the sample collection was operated in an open system that limits its application for experiments that are redox-sensitive or require accurate measurement of volatile components such as H_2, and, in the case of sphalerite, H_2S.

In natural hydrothermal fluids, chloride (Cl) is usually the most concentrated ligand, and is widely accepted to account for Zn transport over a large T-P conditions due to the high stability of Zn-Cl complexes (Ruaya and Seward, 1986; Bourcier and Barnes, 1987; Plyasunov and Ivanov, 1990; Hemley et al., 1992; Cygan et al., 1994; Anderson et al., 1998; Brugger et al., 2003; Pokrovski et al., 2005; Akinfiev and Tagirov, 2014; Mei et al., 2015; Zhong et al., 2015). Four Zn-Cl species, namely $ZnCl^+$, $ZnCl_2$(aq), $ZnCl_3^-$ and $ZnCl_4^{2-}$, have been recognized according to recent experimental and theoretical studies (e.g., Akinfiev and Tagirov, 2014; Mei et al., 2015). However, the relative importance of these species under different T-P conditions and fluid compositions is still controversial (Ruaya and Seward, 1986; Bourcier and Barnes, 1987; Cygan et al., 1994; Sverjensky et al., 1997; Liu et al., 2007; Akinfiev and Tagirov, 2014; Mei et al., 2015). The experimental studies of Ruaya and Seward (1986) and Bourcier and Barnes (1987) point out that $ZnCl_3^-$ and $ZnCl_4^{2-}$ are predominant in fluids (>0.1 m Cl) up to 300 °C, whereas above 300 °C, the stability of $ZnCl_3^-$ and $ZnCl_4^{2-}$ decreases dramatically and $ZnCl_2$(aq) becomes the predominant species. In contrast, two recent studies by Akinfiev and Tagirov (2014) and Mei et al. (2015) suggest that $ZnCl_3^-$ and $ZnCl_4^{2-}$ are predominant species in Cl-dominant fluids at temperatures up to 400 °C. Nevertheless, species with less Cl are likely to be important at higher temperatures, e.g., >400 °C (Seward and Barnes, 1997; Brugger et al., 2016). For example, Cygan et al. (1994) suggests that $ZnCl^+$ and $ZnCl_2$(aq) are the predominant species at 300–600 °C, 0.5–2 kbar, and with 0.25–2 m Cl in fluids. As a result of the different interpretations of Zn speciation in the experimental solutions, the stability constants for Zn-Cl species reported in different studies show significant inter-study differences, especially at elevated temperature, i.e., >350 °C (e.g., Plyasunov and Ivanov, 1990; Cygan et al., 1994; Sverjensky et al., 1997; Akinfiev and Tagirov, 2014; Mei et al., 2015), which obviously limits the understanding of Zn transport in hydrothermal systems.

In the present study, we measured the solubility of sphalerite in acidic NaCl-H_2O solutions at 300–450 °C, 500 bar conditions that are directly relevant for seafloor hydrothermal systems. We designed a new gas-tight titanium (Ti) piston sampler that enables sampling of fluid while maintaining its *in-situ* composition at high T-P conditions. We found that the predicted stability of chloride complexes from Mei et al. (2015) reproduces the experimental trends well, but not the total concentrations at high temperature in 500 bar experiments. A revision of the thermodynamic properties of Zn^{2+} enables the model to cover the extended range in experimental conditions to fluids of relatively low density (≥0.35 g/cm^3). The new data were applied for thermodynamic simulation of Zn transport in a rock-buffered system to better constrain factors controlling Zn transport in natural hydrothermal systems, particularly at deep sea vents.

2. METHODS

2.1. Reactor preparation

The experiments were performed using a fixed volume (165 ml) Ti reactor (Fig. 1a) made of the high-strength Ti-6Al-2Sn-4Zr-2Mo (Ti6242) alloy, that is suitable for high temperature–pressure experiments up to 500 °C, 500 bar (Scheuermann et al., 2018b; Fowler et al., 2019). The interior surface of the reactor was passivated using 20 wt.% nitric acid at 350 °C for 10 h following the procedure described in Fowler et al. (2019). This passivation process allowed formation of an inert TiO_2(s) coating on all wetted internal surface, so as to inhibit possible reaction with included redox and pH buffers (Shmulovich et al., 2002; Rempel et al., 2012). Fowler et al. (2019) tested the effectiveness of this approach by injecting a known amount of H_2 into a passivated Ti-alloy reactor at 300 °C and 300 bar, and measuring the H_2(aq) concentration periodically over 5 days. Their results show no change in the H_2(aq) concentration within error, indicating that Ti-alloy does not participate in reactions involving H_2(aq) after passivation. H_2 measurements conducted by Scheuermann et al. (2020) using the same apparatus as in the present

Please cite this article in press as: Xing Y., et al. An experimental and thermodynamic study of sphalerite solubility in chloride-bearing fluids at 300–450 °C, 500 bar: implications for zinc transport in seafloor hydrothermal systems. *Geochim. Cosmochim. Acta* (2022), https://doi.org/10.1016/j.gca.2022.03.026

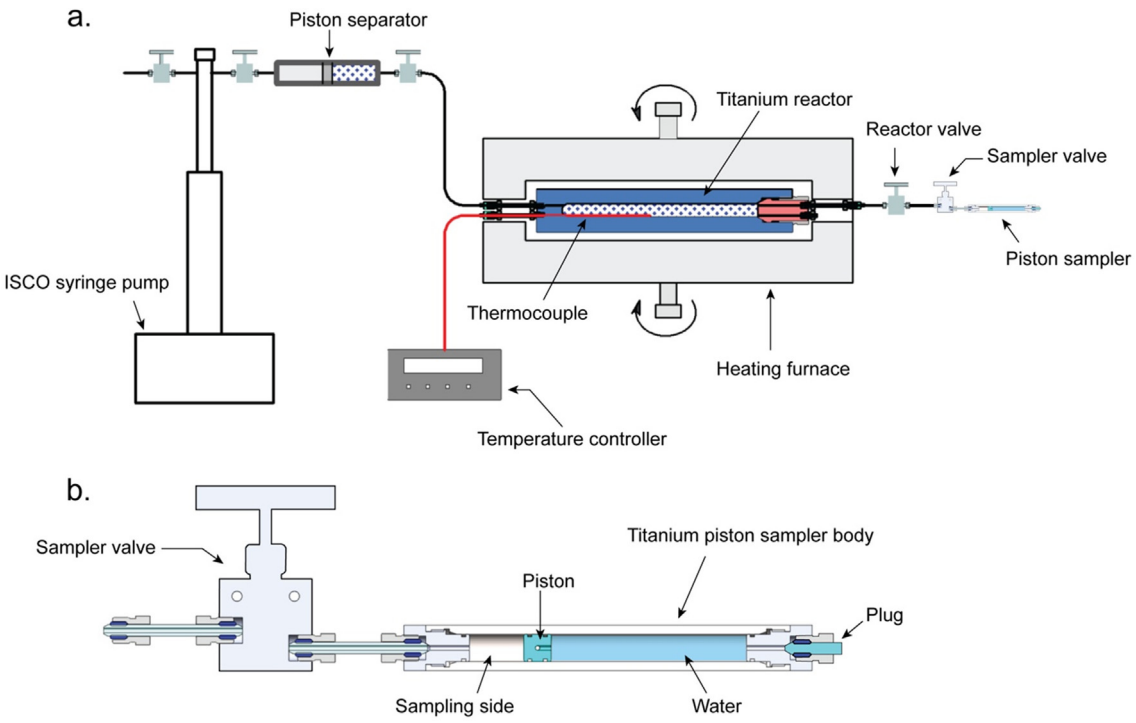

Fig. 1. The experimental setup. (a) Overview of the system for solubility measurements; the piston separator and the Ti reactor are connected using 1/16″ Ti capillary tubing. Modified after Fowler et al. (2019) and Scheuermann et al. (2018b). (b) A detailed illustration of the gas-tight Ti piston sampler. The sampling side of the sampler is loaded with 2 m HCl solution to avoid Zn precipitation, whereas the other side of the sampler is loaded with water to monitor the volume.

study and an overall similar timeframe further support the effectiveness of the passivation layer in slowing down H_2 diffusion.

2.2. Hydrothermal experiments

Natural, gem quality sphalerite crystals from Cananea Sonova, Mexico were used as starting material of the experiment. X-ray powder diffraction (XRD) spectra of this starting material, fitted via quantitative Rietveld method (Rietveld, 1969), show that the sphalerite is > 99% pure (Supplementary Fig. S1; reference sphalerite structure data was from the COD database, phase ID: 9000107). Starting solutions with 0.5 m and 1 m NaCl were prepared using deionized water and reagent-grade NaCl. The solution pH was monitored at ~ 2.5 at 25 °C by addition of ultrapure concentrated HCl acid. We loaded 5 g of sphalerite that was crushed into smaller pieces (<5 mm in diameter) into the reactor to ensure sufficient Zn for the reaction. The starting NaCl solution was flushed using Ar gas for 30 min after loading into the reactor to remove dissolved O_2. A 1/16″ Ti-sheathed type E thermocouple (Chromel-Constantan) was inserted into the reactor to measure the solution temperature (Fig. 1a). The thermocouple has an accuracy of ± 1.5 °C and was calibrated before the experiment using a dry block probe calibrator (Omega Hot Point®). A Thermcraft e-XPRESS-LINE furnace was used for heating. The reactor was connected to a 500 ml in-line Ti piston separator which was filled with the starting solution on one side to buffer the volume change of solutions inside the reactor upon heating. The other side of the separator was filled with deionized water and connected to a Teledyne ISCO syringe pump that can automatically control the system pressure (±2 bar).

The experiments were performed isobarically at 500 bar over a temperature range of 300–450 °C. The experiments initially started from 300 °C. The reaction equilibrium was reached rapidly (<1 h) at high temperatures for Zn sulfide in acidic NaCl solutions (Barrett and Anderson, 1982; Bourcier and Barnes, 1987). A recent study by Murcia et al. (2017) on sphalerite solubility also reported that for experiments conducted even at low temperatures (i.e., 40–80 °C), equilibrium can be achieved within 72 h. For our experiments, we allowed 7 days to ensure equilibrium was achieved at each temperature, with two samples collected sequentially within 2–3 days.

2.3. Sampling using a newly designed gas-tight sampler

The newly designed gas-tight Ti piston sampler has a total volume of 20 ml, and integrates an internal Ti piston to monitor the amount of sample to be collected (Fig. 1b). For sample collection, the sampling side of this device was filled with ~ 3.5 ml 2 m HCl solution to avoid Zn precipitation. The sampler was weighed to accurately determine the amount of acid loaded. The opposite side of the piston was filled with water to balance the volume and was sealed with a Ti pressure plug.

Please cite this article in press as: Xing Y., et al. An experimental and thermodynamic study of sphalerite solubility in chloride-bearing fluids at 300–450 °C, 500 bar: implications for zinc transport in seafloor hydrothermal systems. *Geochim. Cosmochim. Acta* (2022), https://doi.org/10.1016/j.gca.2022.03.026

Before sampling, we flushed ~ 0.3 g fluid from inside of the reactor to clean the capillary line. During sampling, a sample was first collected via the reactor valve for pH measurement and anion analysis. The sampler was then connected to a gas-tight two-way Ti valve (sampler valve, Fig. 1b), which was further connected to the reactor valve attached to the reactor (Fig. 1a). The reactor valve was connected to the reactor using 1/16″ Ti capillary tubing. The sampler valve was fully opened each time before we quickly opened the reactor valve. The high pressure inside the reactor ensured rapid passage of the solution into the sampler, where the sample mixed with the pre-loaded acid solution. Subsequently, both sampler valve and reactor valve (Fig. 1a) were closed, and the sampler valve was detached from the reactor valve. The sampler was then weighed to obtain the total amount of the solution mixture. A mixing ratio was calculated based on the acid solution added and the sample fluid collected. Fluid collected in the sampler was sealed by the gas-tight valve (Fig. 1b). We used another ISCO pump, which was connected to the other side of the sampler (by removing the pressure plug shown in Fig. 1b), to pump out the mixed sample solution via the sampler valve. A gas-tight syringe was used to collect the sample for H_2S(aq) analysis.

2.4. Analytical methods

Concentrations of Zn and Na were measured using inductively coupled plasma optical emission spectroscopy (ICP-OES). Each measurement was repeated four times and an average value was reported. Uncertainty for the ICP-OES analysis is ± 3%. The $pH_{25°C}$ of sample solution was measured using a ThermoRoss microelectrode, which has an uncertainty of ± 0.1 pH units. The pH electrode was calibrated using standard pH buffers with $pH_{25°C}$ 4, 7, and 10 before each measurement. The concentration of Cl was analyzed by ion chromatography (IC) with an uncertainty of ± 2%. Concentrations of H_2S(aq) were measured using iodometric titration (EPA Method 9034).

2.5. Thermodynamic modelling

In this work, thermodynamic modelling was conducted using the HCh software package, which uses a Gibbs free energy minimization algorithm to calculate the equilibrium of mineral-fluid systems (Shvarov and Bastrakov, 1999). The thermodynamic properties of aqueous species and minerals were collected from an updated version of the Unitherm database (Shvarov, 1999; Xing et al., 2019b). A list of EoS model and data source of minerals and aqueous species used in the modelling are provided in Table S1.

The activity coefficients of aqueous species were calculated using the extended Debye-Hückel equation for NaCl-dominated solutions (Helgeson et al., 1981; Oelkers and Helgeson, 1990; Oelkers and Helgeson, 1991):

$$\log \gamma_i = -\frac{Az_i^2\sqrt{I}}{1 + B\,å\,\sqrt{I}} + \Gamma_\gamma + b_\gamma I$$

γ_i is the activity coefficient; A and B are the Debye-Hückel solvent parameters; z_i is the ionic charge; å is the is the ion size; I is the effective ionic strength; Γ_γ is the molarity to molality conversion factor; b_γ is the extended-term parameter for NaCl-dominated solutions from Oelkers and Helgeson (1990), which is a function of temperature (Helgeson, 1969).

3. RESULTS AND DATA TREATMENT

3.1. Measured solubility of sphalerite

The fluid chemistry data are summarized in Table 1. The chemical composition of fluids collected at the same conditions and from different direction in T-P space were reproducible, confirming that fluid-mineral equilibrium was achieved. The measured Zn concentrations increase with increasing temperature for experiments conducted in both 0.5 m and 1 m NaCl solutions (Table 1; Fig. 2). The concentrations of H_2S(aq) were measured as an additional constraint of Zn solubility. For each sample, H_2S(aq) concentration was found close to the measured Zn concentration (Fig. 2). These results indicate that sphalerite dissolved congruently, such that the sphalerite solubility reaction in our experiments can be expressed as:

$$ZnS(s) + 2H^+ + n\ Cl^- = ZnCl_n^{2-n}(aq) + H_2S(aq) \quad (1)$$

where n represents numbers of Cl in the range of 0 ~ 4.

We calculated the sphalerite solubility (reaction (1)) and Zn speciation in NaCl-HCl-H_2O fluids simulating our experimental conditions at 300–450 °C, 500 bar. The amounts of HCl in the starting fluids were set for fluids to have a calculated $pH_{25°C}$ equal to the average measured $pH_{25°C}$ at each temperature (Table 3). Thermodynamic data of aqueous Zn species, in particular Zn chloride complexes, are available from multiple sources that can be used to interpret Zn solubility and speciation (Sverjensky et al., 1997; Akinfiev and Tagirov, 2014; Mei et al., 2015). Accordingly, these data allow examination of the experimental data, and vice versa. In our model, thermodynamic data of Zn-Cl species, $ZnCl^+$, $ZnCl_2$(aq), $ZnCl_3^-$, and $ZnCl_4^{2-}$, from various datasets including an updated version of SUPCRT (Johnson et al., 1992; Sverjensky et al., 1997; Shock et al., 1997), Akinfiev and Tagirov (2014) and Mei et al. (2015), were used for comparison. In addition to Zn-Cl species, the model also includes H^+, OH^-, Na^+, Cl^-, HCl(aq), NaCl(aq), NaOH(aq), H_2(aq), O_2(aq), H_2S(aq), HS^-, and Zn-HS species, i.e., $ZnHS^+$, $Zn(HS)_2$(aq), $Zn(HS)_3^-$, and $Zn(HS)_4^{2-}$ (A detailed list of these species is provided in Table S2).

Results show that at 300–400 °C the calculated Zn solubilities based on the datasets involved are in good agreement with the measured values (Fig. 3). Above 400 °C, differences of predicted Zn solubility between data sources become apparent, and the observed variations increase with increasing temperature. Calculation using SUPCRT data predicts solubility values close to the measured data at these conditions, whereas more recent thermodynamic data from Mei et al. (2015) and Akinfiev and Tagirov (2014) predict values higher than measured in the present study, especially at 450 °C.

Please cite this article in press as: Xing Y., et al. An experimental and thermodynamic study of sphalerite solubility in chloride-bearing fluids at 300–450 °C, 500 bar: implications for zinc transport in seafloor hydrothermal systems. *Geochim. Cosmochim. Acta* (2022), https://doi.org/10.1016/j.gca.2022.03.026

Table 1
Composition of experimental solutions.

Sample No.	T (°C)	P (bar)	$pH_{25°C}$	Na (mol/kg)	Error† (%)	Zn (mmol/kg)	Error† (%)	Cl (mol/kg)	H_2S (mmol/kg)
Zn01	300	500	3.06	1.36	1.46	1.47	0.36	1.37	-
Zn03	300	500	2.96	1.33	0.49	1.12	0.22	1.33	1.26
Zn04	350	500	2.91	1.24	1.46	1.23	1.31	1.25	1.05
Zn05	350	500	2.88	1.15	1.13	1.17	1.00	1.17	0.95
Zn06	400	500	2.74	1.16	1.51	1.79	0.38	1.17	1.67
Zn07	400	500	2.71	1.21	2.39	1.88	0.30	1.19	1.56
Zn08	425	500	2.47	1.18	0.77	2.32	0.55	1.18	2.12
Zn09	425	500	2.43	1.16	0.81	2.34	0.54	1.17	2.11
Zn10	450	500	2.36	1.16	3.18	2.72	1.57	1.17	2.55
Zn11	450	500	2.48	1.18	0.7	2.75	0.39	1.17	2.21
Zn14	300	500	4.05	0.52	0.37	0.27	0.50	0.54	0.04
Zn15	300	500	2.82	0.48	1.29	1.57	0.64	0.51	1.50
Zn16	350	500	2.74	0.49	2.18	1.56	1.10	0.51	0.99
Zn17	350	500	2.78	0.51	0.80	1.56	0.67	0.51	1.42
Zn18	400	500	2.74	0.48	1.02	1.72	0.62	0.52	1.65
Zn19	400	500	2.67	0.48	0.91	1.81	1.13	0.50	1.61
Zn20	425	500	2.49	0.49	1.29	2.37	0.95	0.51	2.34
Zn21	425	500	2.51	0.51	0.18	2.31	0.46	0.51	1.92
Zn22	450	500	2.48	0.48	0.77	2.43	0.51	0.52	2.30
Zn23	450	500	2.60	0.50	3.97	2.41	4.41	0.51	2.23

† Errors at 1-σ level, expressed in % of the experimental value.

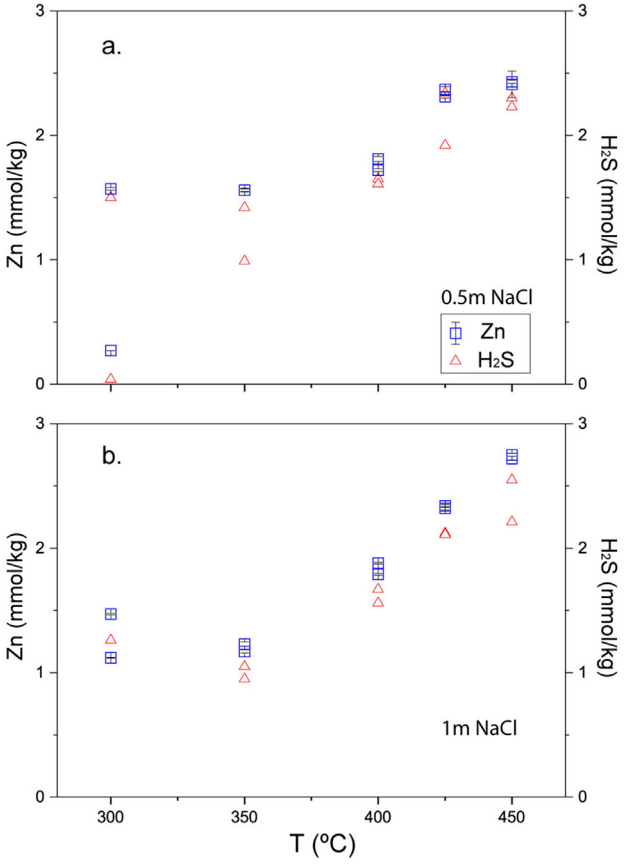

Fig. 2. Concentration of Zn and H_2S for fluids sampled during the experiment. (a) 0.5 m NaCl solution; (b) 1 m NaCl solution.

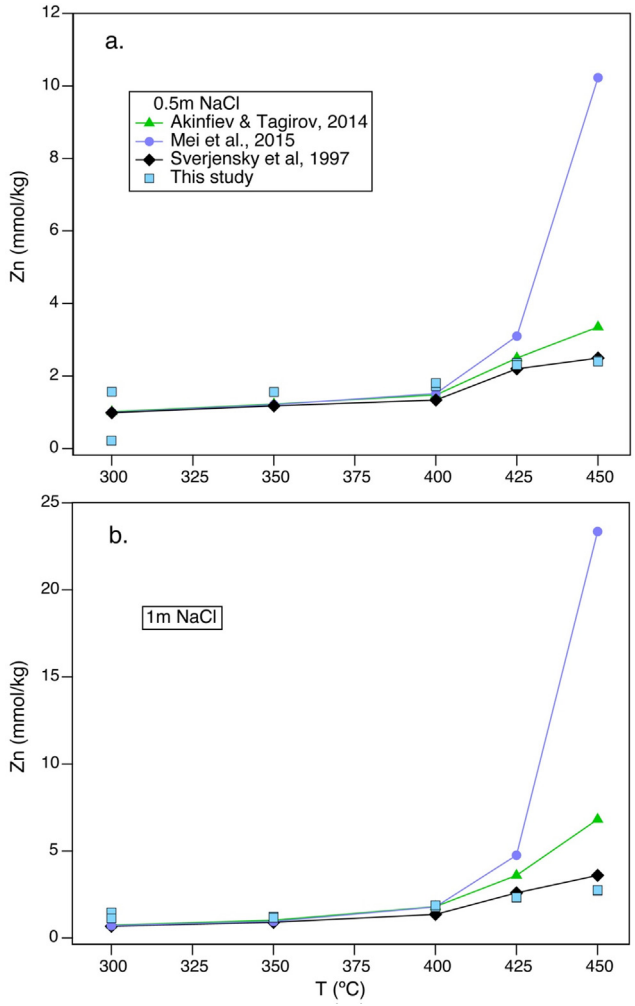

Fig. 3. Zn concentration as a function of temperature in fluids with (a) 0.5 m NaCl solution and (b) 1 m NaCl solution. Note that in (a) one data point at 300 °C shows significantly lower measured Zn, which is a result of a high measured $pH_{25°C}$. This data point was therefore not included in the fitting.

The distribution of Zn species was assessed for NaCl-HCl-H_2O fluids ($pH_{25°C}$ = 2.5) in equilibrium with sphalerite at 300–450 °C and 500 bar, under the same speciation model as above. Results show that Zn speciation varies significantly between datasets. Calculations using the SUPCRT database indicate that $ZnCl^+$ is the predominant species at 300–400 °C; $ZnCl_2$(aq) dominates at above 400 °C; $ZnCl_3^-$ is insignificant at the chemical and physical conditions investigated (Fig. 4a,b). It is noted that SUPCRT does not include $ZnCl_4^{2-}$ because of the large uncertainties among reported thermodynamic data reported for this species (i.e., Ruaya and Seward, 1986; Bourcier and Barnes, 1987), as emphasized by Sverjensky et al. (1997) when they introduced EoS parameters for Zn-Cl species. However, more recent experimental and theoretical studies have demonstrated the importance of $ZnCl_3^-$ and $ZnCl_4^{2-}$ in Cl-rich fluids at elevated temperatures (Anderson et al., 1998; Akinfiev and Tagirov, 2014; Mei et al., 2015). Thus, calculations using the more recent thermodynamic data reported by Akinfiev and Tagirov (2014) and Mei et al. (2015) suggest that $ZnCl_3^-$ and $ZnCl_4^{2-}$ play a dominant role in accounting for Zn solubility (Fig. 4c-f).

3.2. Derivation of thermodynamic model

The apparent inconsistencies in the prediction of Zn solubility and speciation data outlined above underscore the need to better constrain current thermodynamic models, especially at T > 400 °C. Accordingly, we adopted an approach to minimize this discrepancy with the EoS model of Zn-Cl complexes of Mei et al. (2015), because their study (i) benefits from application of a robust model to ~ 350 °C that takes explicit account of internally consistent fit parameters derived from experimental data of Ruaya and Seward (1986) and Bourcier and Barnes (1987); (ii) their speciation scheme is supported by strong evidence from *in-situ* XAS measurements and semi-quantitative *ab initio* MD simulations.

Optimization of the HKF EoS parameters for the Gibbs free energy of formation from the elements ($\Delta_f G^0$) of Zn^{2+}

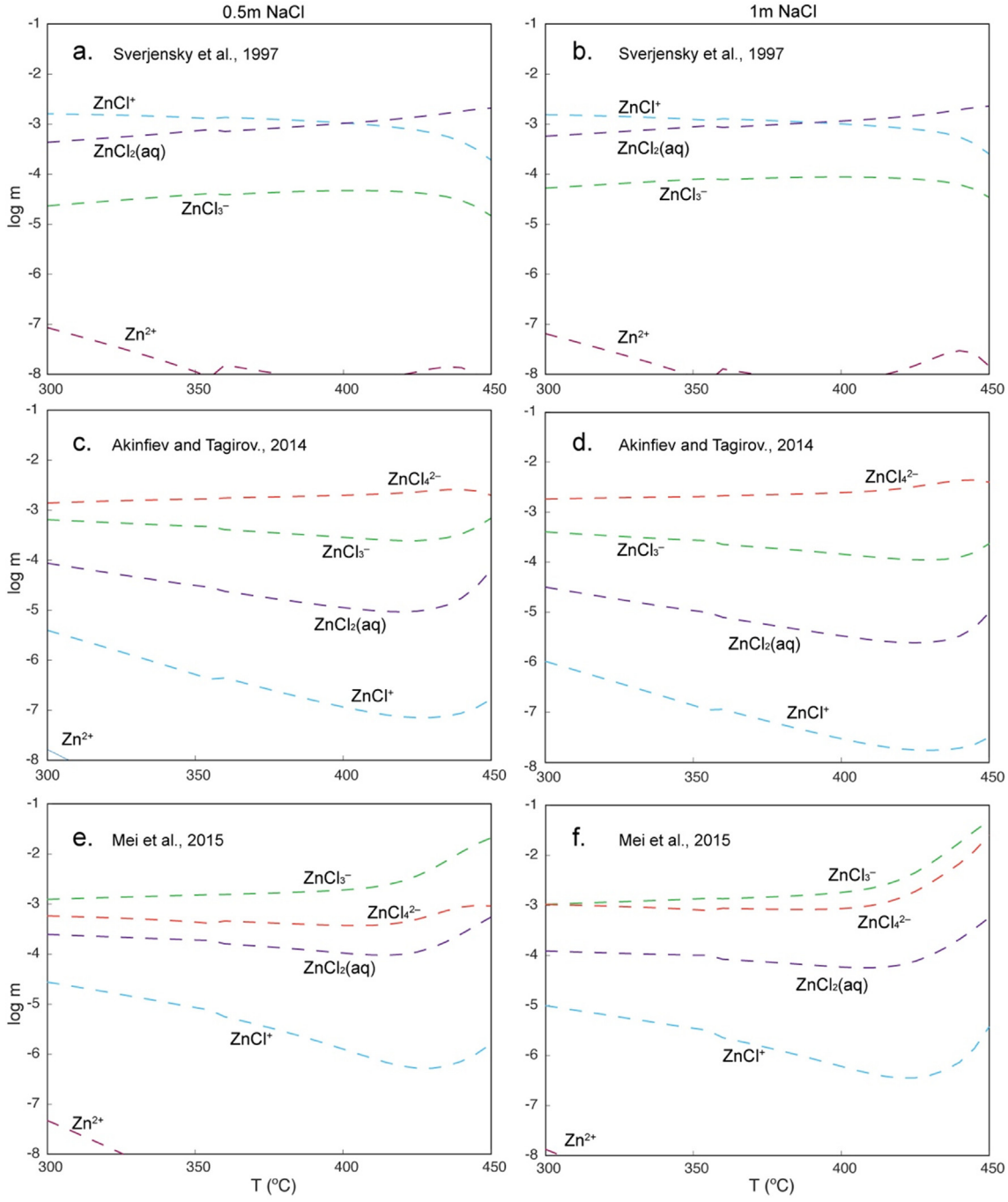

Fig. 4. Calculated Zn speciation for NaCl-HCl-H_2O fluids ($pH_{25°C} = 2.5$) in equilibrium with sphalerite. (a, c, e) Fluids with 0.5 m NaCl. (b, d, f) Fluids with 1 m NaCl. Calculations were performed using thermodynamic data from: (a, b) Sverjensky et al. (1997); (c, d) Akinfiev and Tagirov (2014); and (e, f) Mei et al. (2015).

chloride complexes was firstly performed using the OptimA and OptimB programs (Shvarov, 2015). However, attempts to improve the EoS model by refining the properties of Zn-Cl complexes proved problematic. We used OptimA to obtain $\Delta_f G^0$ for $ZnCl_3^-$ and $ZnCl_4^{2-}$ (fixing properties of $ZnCl^+$ and $ZnCl_2$(aq) from Mei et al. 2015) from a fit of our solubility data at $T \geq 400$ °C. Although good agreement with our experimental data could be obtained in this manner, retaining consistency with a broader range of experimental studies at 100–300 °C required the need for an unacceptably large number of assumptions to constrain data fitting.

We noticed discrepancies between experimental solubility data at 450 °C involving sphalerite (present study), and zincite (Plyasunov and Ivanov, 1990) for calculations performed using Mei et al. (2015)'s model: for both sets

Please cite this article in press as: Xing Y., et al. An experimental and thermodynamic study of sphalerite solubility in chloride-bearing fluids at 300–450 °C, 500 bar: implications for zinc transport in seafloor hydrothermal systems. *Geochim. Cosmochim. Acta* (2022), https://doi.org/10.1016/j.gca.2022.03.026

of experiments, the slope of Zn concentrations as a function of Cl concentrations were well reproduced, but solubilities for both minerals were either overestimated or underestimated (Figs. 3 and 6). This suggests that the stoichiometry of Zn-chloride complexes predicted using Mei et al. (2015) properties is correct, but there is an issue with the predicted solubility products for both sphalerite and zincite at high temperatures:

$$ZnS(s) + 2H^+ = Zn^{2+} + H_2S(aq) \quad (2)$$

$$ZnO(s) + 2H^+ = Zn^{2+} + H_2O \quad (3)$$

Because properties of solids, H^+, $H_2S(aq)$, and H_2O are well established, the solubility product depends chiefly on the properties of the Zn^{2+} aqua ion. Both Akinfiev and Tagirov (2014) and Mei et al. (2015) use thermodynamic data for Zn^{2+} generated by Shock and Helgeson (1988) in the framework of the HKF model based on semi-empirical correlations. We therefore explored whether the HKF parameters of the Zn^{2+} ion could be improved to make the solubility products (2) and (3) consistent with experimental data at 300–450 °C, without significantly affecting the calculations of the Gibbs free energy of formation of Zn^{2+} at lower temperatures (i.e., retaining the self-consistency of the thermodynamic model at T < 300 °C). In these models, we retained the properties for Zn chloride complexes from Mei et al. (2015), and only optimized the Gibbs free energy of formation from the elements for the Zn^{2+} aqua ion. This method works because of the way the thermodynamic properties for the solubility products (equations (2), (3)) and Zn chloride complexes are described in common thermodynamic databases (e.g., HCh, Geochemist's Workbench). Even if Zn^{2+} is a minor species in our experiments, equation (2) defines the background solubility, and each chloride complex increases the solubility. Because Mei et al. (2015) express the changes in Δ_fG^0 of Zn-chloride complexes using the modified Ryzhenko-Bryzgalin (MRB) model for reaction (4), changes in $\Delta_fG^0(Zn^{2+})$ do not affect the predicted relative stabilities of Zn-chloride complexes; in other words, adjusting $\Delta_fG^0(Zn^{2+})$ does not affect the change in slope of sphalerite solubility as a function of activity of the chloride ion, but only increases the total solubility, in a manner consistent with the observed trends between model and experiments.

$$Zn^{2+} + n\ Cl^- = ZnCl_n^{(2-n)} \quad (4)$$

For the final optimization, $\Delta_fG^0(Zn^{2+})$ was calculated by minimizing the difference between the experimental solubility data (300–450 °C) and the solubility calculations using the properties listed in Table S1. HKF parameters were then fitted for $\Delta_fG^0(Zn^{2+})$ using OptimB; in order to ensure that the new $\Delta_fG^0(Zn^{2+})$ were similar to those of Shock and Helgeson (1988) at T ≤ 400 °C, we included $\Delta_fG^0(Zn^{2+})$ at T up to 350 °C (50 °C intervals) calculated from this source in the fitting. The aims of the fit were to find new HKF parameters that provide $\Delta_fG^0(Zn^{2+})$ values that are consistent with Shock and Helgeson (1988)'s values at T ≤ 400 °C (Table S3), ensuring consistency with existing solubility data (listed in Mei et al., 2015), as well as providing a satisfactory agreement with the new experimental data at high temperatures and low pressures (densities down to ~ 0.4 g/cm^3). We found that this could be achieved by fitting the heat capacity (HKF parameters c_1 and c_2) and Born coefficient (HKF parameters ω) while retaining the Δ_fG^0, S^0, and a_1-a_4 values (partial molar volume = f(a_1-a_4)) proposed by Shock and Helgeson (1988). The modified HKF parameters for the Zn^{2+} ion are listed in Table 4, and comparison of $\Delta_fG^0(Zn^{2+})$ values obtained using Shock and Helgeson (1988) and the new HKF parameter are provided in Supp. Table S3. The fit results for sphalerite solubility using the new thermodynamic properties show good agreement with the experimental data of this study (Fig. 5). The speciation calculations show that $ZnCl_3^-$ and $ZnCl_4^{2-}$ are the predominant species over the full range of experimental conditions investigated.

Although the HKF model is designed for solutions with densities ≥ 0.35 g/cm^3, the model can be inaccurate at solvent densities <~0.6 g/cm^3 (e.g., Miron et al., 2019). Our experiments were conducted at minimum density of water ~ 0.40 g/cm^3 (450 °C, 500 bar; Table 2). One reason for the deviations observed might lie in inaccurate estimates for the water solvent dielectric constant and its derivatives; however, the static dielectric constants of water used in the HKF model are reasonably accurate in our experimental domain (within 0.5 of the experimental values selected in Fernández et al., 1995; Table 2). When observing the molar heat capacity and molar volume functions, the new predictions lead to relatively small changes compared to the extrapolations of Shock and Helgeson (1988): the latter predicts rapid changes and results in unrealistic values as density decreases (Fig. S2). Note that it is not surprising the high-T properties of the Zn^{2+} ion are not reproduced accurately by correlative methods; while the hydration of many transition metal complexes changes linearly with decreasing fluid density (e.g., Mei et al. 2014), the Zn^{2+} aqua ion undergoes discrete transitions from octahedral to tetrahedral coordination as temperature increases (Mei et al. 2015; Susak and Crerar, 1985).

3.3. Comparison to previous experimental data

The revised EoS parameters for Zn^{2+} were used to calculate the solubilities of Zn minerals in hydrothermal fluids; these theoretical values are compared with the experimental data reported in previous studies in Fig. 6. The EoS for Zn-Cl species reported in Akinfiev and Tagirov (2014) and Mei et al. (2015) and for Zn^{2+} reported in Shock and Helgeson (1988) were used for comparison. Plyasunov and Ivanov (1990) reported ZnO solubility at 200–600 °C, up to 1000 bar (Table S4), with well reported fluid chemistry. We calculated ZnO solubility at 300 °C, P_{sat}, and 450 °C, 1000 bar in fluids with the same initial fluid chemistry as that of Plyasunov and Ivanov (1990). Results show that at 300 °C, the predicted solubilities are in good agreement at low fluid chlorinities (< 1 m NaCl) with the experimental data, and the difference between datasets are insignificant (Fig. 6a). With increasing chlorinity, predicted values using EoS models of Akinfiev and Tagirov (2014) and Mei et al. (2015) are lower than measured data. At 450 °C, using Mei et al. (2015)'s model for Zn-Cl species provides slightly

Please cite this article in press as: Xing Y., et al. An experimental and thermodynamic study of sphalerite solubility in chloride-bearing fluids at 300–450 °C, 500 bar: implications for zinc transport in seafloor hydrothermal systems. *Geochim. Cosmochim. Acta* (2022), https://doi.org/10.1016/j.gca.2022.03.026

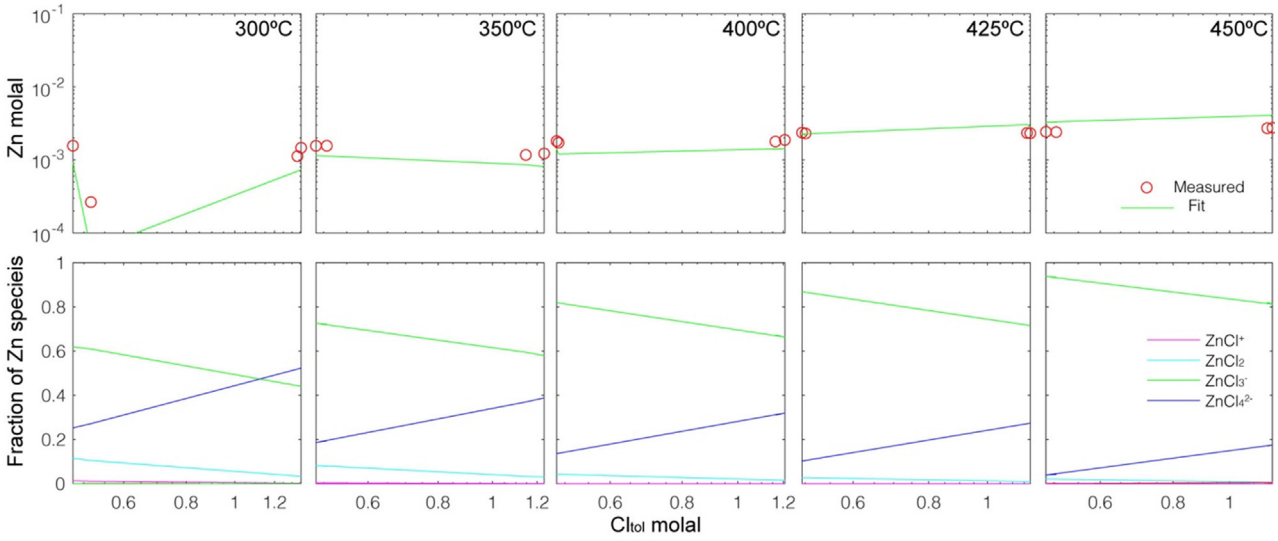

Fig. 5. Comparison of measured solubility data with fitting results. In the upper row of the diagram, measured values of this study are shown in red circles and the fitting results are shown in green lines. The speciation results are shown in the bottom row of the diagram.

Table 2
Water property at 300–450 °C, 500 bar.

T (°C)	P (bar)	ρ H_2O (g/cm^3)	ε
300	500	0.777	23.2
350	500	0.693	17.63
400	500	0.578	12.26
425	500	0.498	9.47
450	500	0.402	6.76

ρ H_2O, density of water; ε, dielectric constant.
Calculated with SUPCRT data in Unitherm.

lower predicted solubility values compared to the experimental data (Fig. 6b). Calculated solubilities using Akinfiev and Tagirov (2014)'s EoS are significantly higher than the measured data at > 0.5 m NaCl (Fig. 6b).

To compare with the experimental data of Cygan et al. (1994), sphalerite solubility was calculated at 300 °C, 500 bar, and 400 °C, 1000 bar in fluids buffered by K-feldspar-muscovite-quartz (KMQ) (Fig. 6c,d; Table S5). The calculation of the solubility curve was performed with a start fluid of $pH_{25°C}$ in a range of 1.5–3.5, thus showing a solubility range in Fig. 6c and 6d. Results show that at both 300 and 400 °C, the calculated ZnS solubilities are close to the experimental data at < 1 m KCl, whereas > 1 m KCl, the predicted values are significantly higher than the experimental values (Fig. 6c,d). The revised Zn^{2+} EoS data improve the simulation quality especially at higher salinities in comparison with predictions based on the Zn^{2+} EoS parameters of Shock and Helgeson (1988).

4. DISCUSSION

4.1. Advancement of sampling technique of high T-P fluids

Mineral solubility experiments at elevated temperature and pressure are critical for understanding hydrothermal processes intrinsic to the formation of hydrothermal ore deposits, 'Black Smoker' growth, fluid circulation in the ocean and continental crust, and large-scale crustal metamorphism and alteration (Ruaya and Seward, 1986; Seyfried et al., 1987; Hemley et al., 1992; Mountain and Seward, 2003; Stefánsson and Seward, 2004; Migdisov et al., 2009; Tagirov and Seward, 2010; Hurtig and Williams-Jones, 2014; Migdisov and Williams-Jones, 2014; Scheuermann et al., 2018a; Fowler et al., 2019; Gysi and Harlov, 2021). Transition metal solubility under these conditions can be dramatically different to those at low temperatures, partly attributed to changes of metal complexing behavior (Brugger et al., 2016). Accurate measurement of metal solubility at high T-P is unusually challenging because of the sensitivity of metal complexes and mineral precipitation to small changes in temperature, pressure, and fluid chemistry makes it difficult to predict the effects of quenching. Since *in-situ* measurements remain limited and are associated with their own sources of uncertainty (e.g., Liu et al., 2008; Brugger et al., 2010; Schmidt et al., 2018; Tagirov et al., 2019), improvements in sampling techniques are crucial for reducing these and other uncertainties and increasing the reliability of solubility data.

Diverse methods have been developed to attempt to recover the *in-situ*, high T-P compositions of sampled solutions, including: gold-cell hydrothermal reactor (Seyfried et al., 1979, 1987; Syverson et al., 2018; Scheuermann et al., 2019), rapid quenching of gold/platinum capsules or quartz glass tubes (Seward, 1976; Ruaya and Seward, 1986; Plyasunov and Ivanov, 1990; Cygan et al., 1994; Akinfiev and Tagirov, 2014), direct sampling of fluid from stainless steel or titanium autoclaves (Bourcier and Barnes, 1987; Scheuermann et al., 2018b), and flow-through reactors (Tagirov et al., 2007; Tagirov and Seward, 2010). Experiments using gold/platinum capsules with rapid quench procedures were often based on the assumption that the quench rate is sufficient to avoid back

Please cite this article in press as: Xing Y., et al. An experimental and thermodynamic study of sphalerite solubility in chloride-bearing fluids at 300–450 °C, 500 bar: implications for zinc transport in seafloor hydrothermal systems. *Geochim. Cosmochim. Acta* (2022), https://doi.org/10.1016/j.gca.2022.03.026

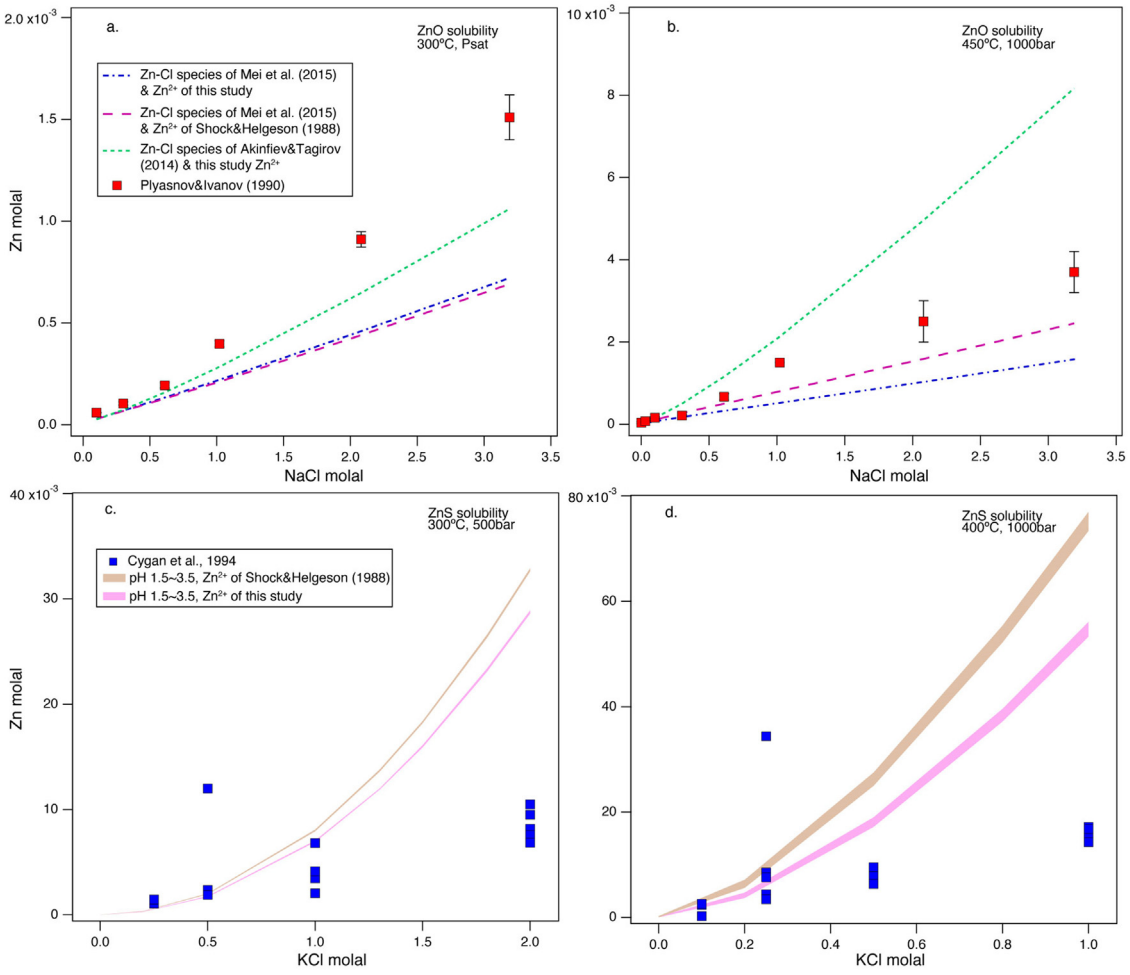

Fig. 6. Solubilities of zincite (ZnO) and sphalerite (ZnS) in Cl-dominant fluids. (a) and (b) show the solubilities of ZnO in NaCl-H_2O solutions at 300 °C, P_{sat}, and 450 °C, 1000 bar, respectively. For (a-b), experimental data for ZnO solubility by Plyasunov and Ivanov (1990) are shown in red squares; ZnO Solubility curves predicted using thermodynamic data of Zn-Cl complexes reported by Akinfiev and Tagirov (2014), or by Mei et al. (2015), with EoS of Zn^{2+} from either Shock and Helgeson (1988) or this study, are plotted in dashed lines for comparison. (c) and (d) show the solubilities of sphalerite at 300 °C, 500 bar and 400 °C, 1000 bar, respectively, in KCl-HCl-H_2O solutions equilibrated with KMQ pH buffer. Experimental data by Cygan et al. (1994) are plotted for comparison. In (c-d), coloured area shows calculated ZnS solubility range in fluid with $pH_{25°C}$ in range of 1.5–3.5, with thermodynamic data of Zn-Cl species from Mei et al. (2015), and Zn^{2+} from either Shock and Helgeson (1988) or this study.

reaction (Hemley et al., 1992; Cygan et al., 1994). In cases where precipitation occurs, procedures for target mineral re-dissolution are applied, often leading to uncertain results. The gold cell reactor enables the collection of *in-situ* high T fluids, but the total volume of the reactor is limited, not suitable for multiple samplings in prolonged experiments; and the cooling of quench solution along the sampling line may result in significant sulfide mineral precipitation, with corresponding uncertainty on inferred metal solubility. The flow-through reactor method greatly improves the sampling reliability by placing the sampling tubing in an adjacent furnace to avoid cooling effects (Tagirov et al., 2007; Tagirov and Seward, 2010). However, collecting samples in an open system exposed to atmosphere enhances the likelihood of redox and fluid composition changes associated with the loss of volatile components.

The Ti-alloy reactor equipped with the newly designed titanium piston sampler features significant advantages for the above high T-P applications: it enables sampling of high T-P solution *in-situ* in a gas-tight manner, with little or no loss of mass via precipitation or degassing; as well as efficient separation of fluids from the buffering solids (Fig. 1). Moreover, mineral precipitation can be further avoided inside the sampler itself by addition of an acid solution. The backpressure regulator helps maintain dissolved gases in solution (Fig. 1b), the loss of which would have a deleterious effect on redox-sensitive species. In effect, this also simplifies sample processing procedures, because the sampler also serves as a mixing and digestion vessel and the collected solution can thus be easily diluted for cation and/or anion analysis. The titanium gas-tight valve attached to the sampler provides a high-pressure seal, making sample collection suitable for analysis of volatile or

Please cite this article in press as: Xing Y., et al. An experimental and thermodynamic study of sphalerite solubility in chloride-bearing fluids at 300–450 °C, 500 bar: implications for zinc transport in seafloor hydrothermal systems. *Geochim. Cosmochim. Acta* (2022), https://doi.org/10.1016/j.gca.2022.03.026

Table 3
Calculated sphalerite solubilities (reported as Zn concentrations) in NaCl-HCl-H_2O solutions at 300–450 °C, 500 bar.

T (°C)	$pH_{25°C}$		Zn (mmol/kg)	
0.5 m NaCl				
300	2.82	0.99	1.00	1.02
350	2.76	1.18	1.21	1.23
400	2.71	1.34	1.52	1.48
425	2.5	2.20	3.10	2.50
450	2.54	2.50	10.23	3.35
1 m NaCl				
300	3.01	0.68	0.71	0.74
350	2.9	0.90	0.95	1.02
400	2.73	1.36	1.79	1.80
425	2.45	2.59	4.76	3.60
450	2.42	3.60	23.36	6.82
Thermodynamic data source of Zn-Cl complexes		SUPCRT	Mei et al., 2015	Akinfiev and Tagirov, 2014

Note: Details of thermodynamic data used for the calculations are listed in Table S1.

Table 4
Parameters of HKF model derived for Zn^{2+}.

HKF parameters	Zn^{2+}
$\Delta_f G^0$, cal ·:	−35200
$\Delta_f H^0$, cal:	−36660
S^0, cal · K^{-1}:	−26.2
V^0, cm^3 mol^{-1}	**−24.3** (-21.2)
C_p^0, cal mol^{-1} K^{-1}	**6.6** (-6.3)
a_1*10, cal mol^{-1} bar^{-1}	−1.0677
a_2*10^{-2}, cal mol^{-1}	−10.3884
a_3, cal K mol^{-1} bar^{-1}	9.8331
a_4*10^{-4}, cal K mol^{-1}	−2.3495
c_1, cal mol^{-1} K^{-1}	**−13.4576** (15.9009)
c_2*10^{-4}, cal K mol^{-1}	**10.8697** (-4.3979)
ω*10^{-5}, cal mol^{-1}	**0.2175** (1.4574)
z	2

Note: parameters in bold were optimized; values in parenthesis are the original values according to Shock and Helgeson (1988).

redox-sensitive components such as H_2(aq) and H_2S(aq). These advances greatly improve the reliability of solubility experiments.

4.2. Zn transport in Cl-bearing hydrothermal fluids

The improved HKF parameters for Zn^{2+} present an opportunity to better constrain Zn solubility and speciation in Cl-dominant fluids at elevated T-P conditions. Factors such as temperature, chlorinity, and pH are known to affect Zn transport in hydrothermal fluids (Ruaya and Seward, 1986; Mayanovic et al., 1999; Harris et al., 2003; Akinfiev and Tagirov, 2014; Mei et al., 2015). Among all, temperature commonly plays a key role in determining hydrothermal mobility of Zn in nature; as shown by our experimental data, sphalerite solubility increases towards higher temperature (Figs. 2 and 3; Table 1), a fact also reflected in the analyses of natural hydrothermal waters (Yardley, 2005). The combining effects of fluid pH and chlorinity are illustrated with a simplified model by calculating sphalerite solubility in NaCl-HCl-H_2O fluids (Fig. 7; Table S7). The starting fluids have a specified calculated $pH_{25°C}$ by adjusting the HCl concentration at the beginning. The speciation model is the same as that shown in Table S2 with Zn-Cl species of Mei et al. (2015) and Zn^{2+} of this study. Results show that with increasing initial fluid $pH_{25°C}$, the solubility of sphalerite (expressed as total dissolved Zn) decreases (Fig. 7). Fluids with higher Cl concentrations are capable of dissolving higher amounts of Zn (Figs. 6 and 7). However, the effect of chlorinity is more significant at higher fluid pH (Fig. 7). We suggest that this is caused by the fact that at elevated temperature, the effects of *in-situ* pH on Zn solubility decreases as a result of strong complexation of HCl(aq) (Tagirov et al., 1997; Ho et al., 2001; Mei et al., 2018), such that the formation of high-order Zn chloride complexes becomes relatively more important in controlling Zn solubility. The experimental data from Cygan et al. (1994) indicate similar trends (Fig. 7; Table S6), in that fluids with lower quench pH contain higher Zn concentrations, and the variation of salinity plays a negligible role on Zn solubility at low pH (Fig. 7a, b). Although the predicted (revised) sphalerite solubilities are generally in agreement with the experimental data of Cygan et al. (1994), it is observed that the data of Cygan et al. (1994) show a slight shift from the predicted values. This may be the result of a pH shift caused by mineral precipitation and/or associated reactions upon quenching of the experiment. Cygan et al. (1994) acknowledge that such problems can cause the experimental data to be equivocal and hence require further study, especially for a complex rock-buffered system.

Further speciation calculations were performed to reveal Zn speciation in response to T-Cl-pH (Fig. 8). The results confirm the predominance of $ZnCl_3^-$ and $ZnCl_4^{2-}$ in fluids with moderate chlorinity (≥seawater) and more acidic conditions at high temperatures (>300 °C), consistent with previous studies (Bourcier and Barnes, 1987; Akinfiev and Tagirov, 2014; Mei et al., 2015). $ZnCl_2$(aq) and/or Zn-HS complexes (Etschmann et al., 2019) are predominant in fluids with low Cl concentrations. Particularly, Zn-HS complexes are predominant in fluids with higher pH (Fig. 8a).

4.3. Zinc transport in seafloor hydrothermal systems

Vent fluids from seafloor hydrothermal systems have Zn concentrations from 1 μmol/kg to > 400 μmol/kg (Edmonds et al., 1996; Gamo et al., 1996; Seyfried et al., 2003; Ji et al., 2017; McDermott et al., 2018), which almost certainly results from fluid-rock equilibria at a range of physical and chemical conditions (e.g., de Ronde et al., 2011). To better understand Zn transport in these systems, we performed thermodynamic modelling using the new thermodynamic data in a simplified rock-buffered system, which has KMQ as the buffer pH, and hematite + magnetite (HM) or pyrite + pyrrhotite + magnetite (PPM) assemblages as redox controls, respectively. In seafloor hydrothermal systems, basalt is the predominant host rock (Seyfried and Mottl, 1982; Seyfried and Ding, 1995).

Please cite this article in press as: Xing Y., et al. An experimental and thermodynamic study of sphalerite solubility in chloride-bearing fluids at 300–450 °C, 500 bar: implications for zinc transport in seafloor hydrothermal systems. *Geochim. Cosmochim. Acta* (2022), https://doi.org/10.1016/j.gca.2022.03.026

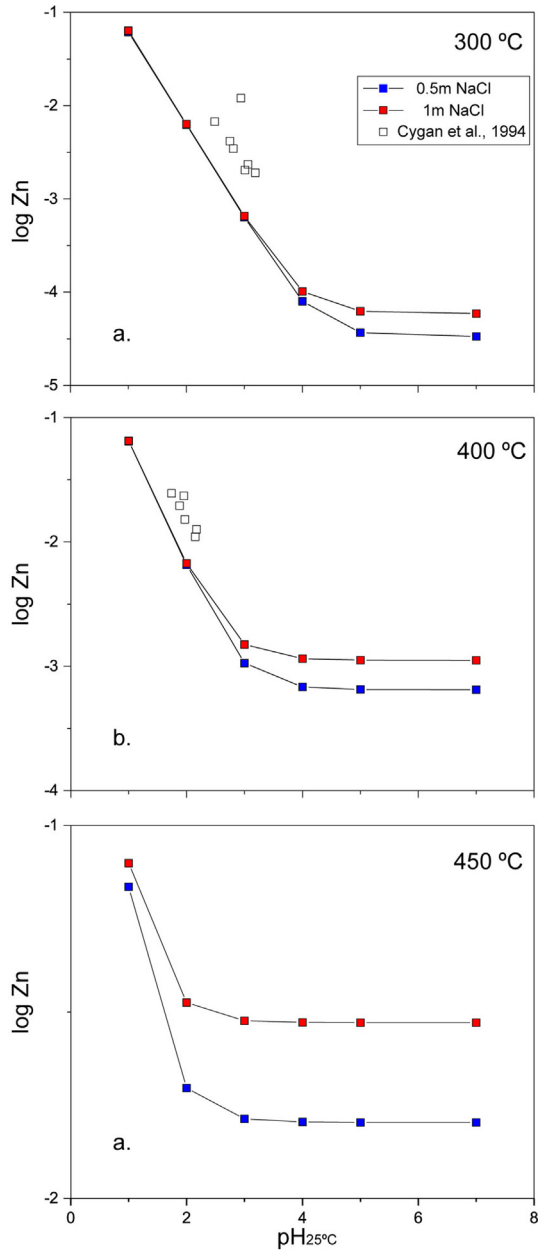

Fig. 7. Calculated sphalerite solubility as a function of $pH_{25°C}$ for fluids containing 0.5 m and 1 m NaCl. (a) 300 °C, (b) 400 °C and (c) 450 °C. Experimental data from Cygan et al. (1994) on sphalerite solubility in fluids with 0.5 m and 1 m KCl (not specifically distinguished in the diagram here due to insignificant influence from salinity at logarithmic scale) at 300 °C and 400 °C, 500 bar, are plotted for comparison for fluids against reported quenched pH.

Although K-feldspar is a minor component in basalt, the KMQ pH buffer is widely used experimentally or theoretically to cover the range of pH values typical of complex basalt-hosted alteration by adjusting the activity of dissolved K^+ (Foustoukos and Seyfried, 2005; Scheuermann et al., 2020; Xing et al., 2021), as was the case here. It is also noted that in this modelling, sufficient sphalerite was included as the Zn source to avoid the complexity of fluid/rock ratio that potentially affects metal solubility such as in many natural hydrothermal systems (e.g., Thébaud et al., 2008; Meffre et al., 2016; Xing et al., 2018; Xing et al., 2019a). Calculations were performed using the aliquot-type model as detailed in Xing et al. (2019b); the simulated conditions were 250–450 °C, 500 bar, and the fluid salinity range was 0–2 m NaCl. Hence these calculations illustrate the effects of temperature, chlorinity and redox conditions, though in a system saturated with sphalerite, with broad implications in rock buffered mineralizing systems over a wide range of temperature and salinity.

Results show that both fluid chlorinity and temperature have significant influences on Zn solubility (Fig. 9). The Zn solubility in fluids with HM redox buffer is overall higher than the PPM buffer, indicating that oxidized conditions favor Zn transport. Zn chloride complexes, especially $ZnCl_3^-$ and $ZnCl_4^{2-}$, are the predominant species over most of the simulated T-Cl range, whereas $ZnCl_2$(aq), Zn-OH and Zn-HS species are important only in low-Cl fluids and/or at higher pH.

In natural hydrothermal systems, including the seafloor vents, fluid/rock ratio is also an important factor determining observed fluid chemistry and base metal-bearing mineralization (Bau, 1991; Alt-Epping and Smith, 2001; German and Seyfried, 2014; Xing et al., 2018; Xing et al., 2019a). Hence, temperature, salinity, pH, as well as fluid/rock ratio, should function as a whole, contributing to the observed metal contents. Accordingly, we modelled fluid-basalt reaction with varying fluid/rock ratios in order to provide some preliminary constraints on such processes. The composition of basalt in the model was taken based on the average Mid-Ocean-Ridge basalt (MORB) composition reported in Gale et al. (2013), which has 91.3 ppm Zn (Table S8). Systems with fluids containing 0.5 m and 1 m NaCl, and with fluid/rock ratio of 1 and 10 were calculated. The results were compared with the saturated sphalerite solubilities in a KMQ pH buffer (Fig. 10). As observed from the modelling results, higher fluid/rock ratio results in lower Zn concentrations. Fluids with higher chlorinity favor Zn transport, potentially depleting the full inventory of basalt-derived Zn, as shown by the flattening of the Zn concentration lines in Fig. 10. In cases where basalt reaches its buffering limit for Zn (e.g., towards higher temperature), subsequent changes in chlorinity and/or temperature have insignificant effects on Zn solubility (Fig. 10).

Data for high temperature brine fluids from the Brandon vent (368–376 °C, 557–558 mmol/kg Cl) along the East Pacific Rise (21.5°S, EPR; Von Damm et al., 2003), the Rainbow hydrothermal system (>350 °C, ~700 - ~760 mmol/kg Cl) at Mid-Atlantic Ridge (36°N, MAR; Seyfried et al., 2011), TAG hydrothermal mound at MAR 26°N (Edmonds et al., 1996), and Kairei and Edmond (273–382 °C, ~570-~930 mmol/kg) at Central Indian Ridge (23-25°S, Gallant and Von Damm, 2006) show dissolved Zn concentrations well undersaturated with respect to sphalerite at chemical and physical conditions appropriate for fluids issuing from these vent systems (Fig. 10). It should be noted that this is a rough comparison since the model here provides a maximum estimate of Zn solubility through simple equilibrium calculations, yet in reality significant

Please cite this article in press as: Xing Y., et al. An experimental and thermodynamic study of sphalerite solubility in chloride-bearing fluids at 300–450 °C, 500 bar: implications for zinc transport in seafloor hydrothermal systems. *Geochim. Cosmochim. Acta* (2022), https://doi.org/10.1016/j.gca.2022.03.026

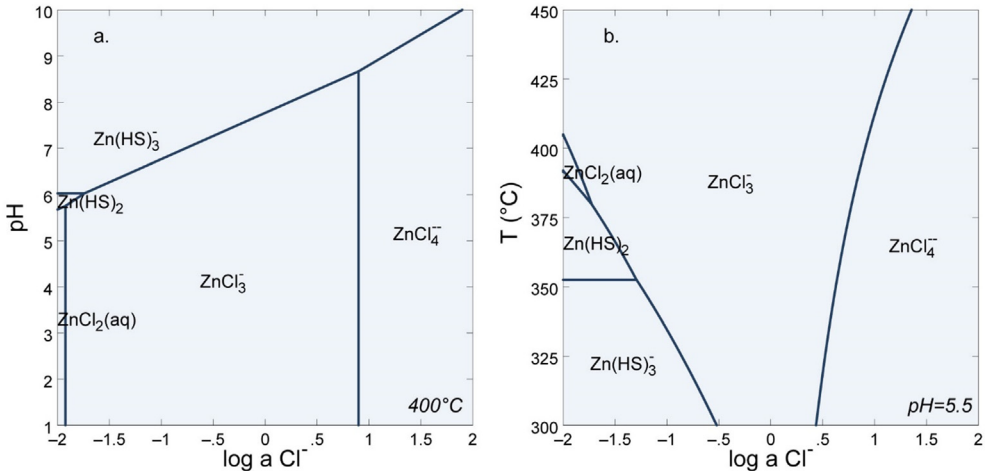

Fig. 8. Speciation of Zn as a function of Cl activity, pH and temperature. (a) pH-Cl diagram at 400 °C; (b) T-Cl diagram at pH = 5.5. Both calculations were performed at 500 bar, in the presence of log $a(H_2S)_{aq} = -2$. Calculation was performed using the Geochemist's Workbench (GWB) software (Bethke, 2007).

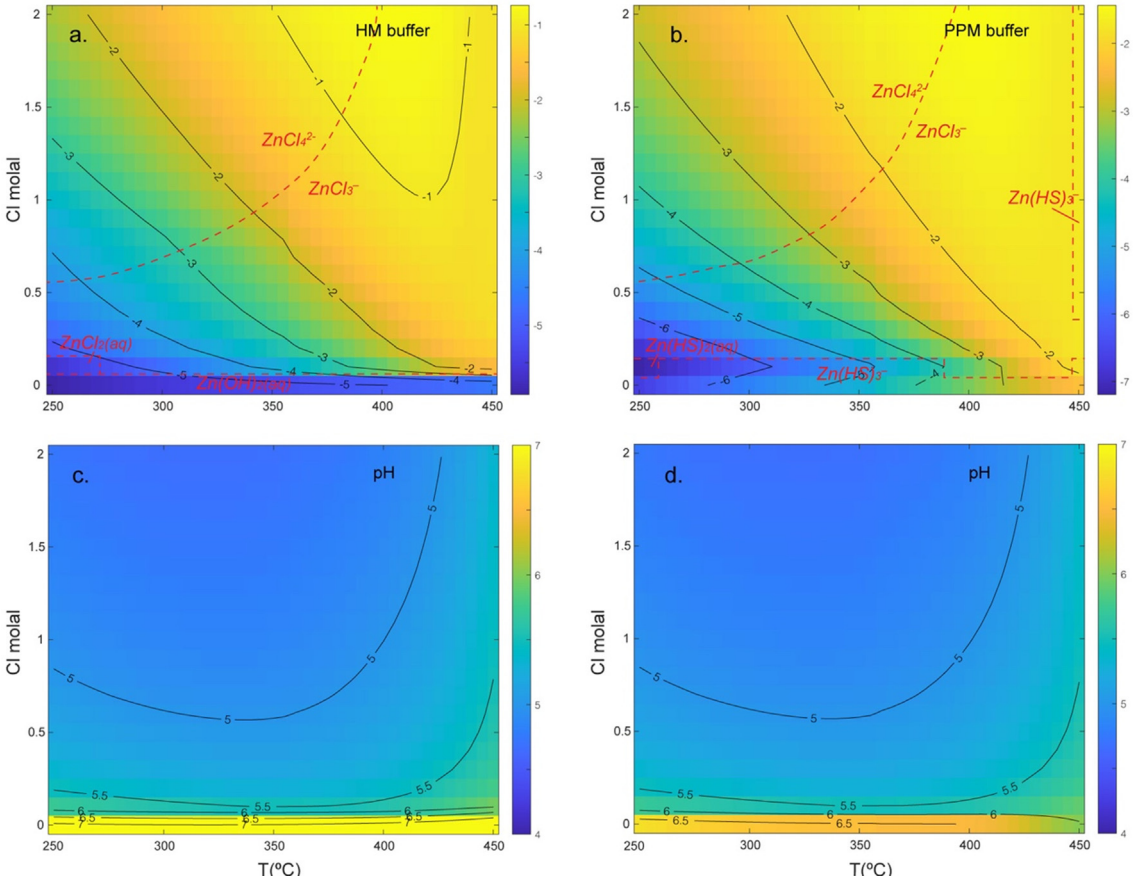

Fig. 9. Calculated Zn concentration and fluid pH as a function of temperature and fluid salinity in rock buffered systems. (a, c) show Zn concentration and fluid pH for KMQ-HM buffered system. (b, d) show Zn concentration and fluid pH for KMQ-PPM buffered system. Black lines represent molal Zn concentration (in logarithm) contours in (a, b), while in (c, d) represent pH contours. Red dashed lines in (a) and (b) show the boundaries of predominant aqueous Zn species. The names of the predominant Zn species are shown in red color text next to the boundary lines. Colored scale bar indicates Zn solubility range in (a, b); and pH range in (c, d).

Please cite this article in press as: Xing Y., et al. An experimental and thermodynamic study of sphalerite solubility in chloride-bearing fluids at 300–450 °C, 500 bar: implications for zinc transport in seafloor hydrothermal systems. *Geochim. Cosmochim. Acta* (2022), https://doi.org/10.1016/j.gca.2022.03.026

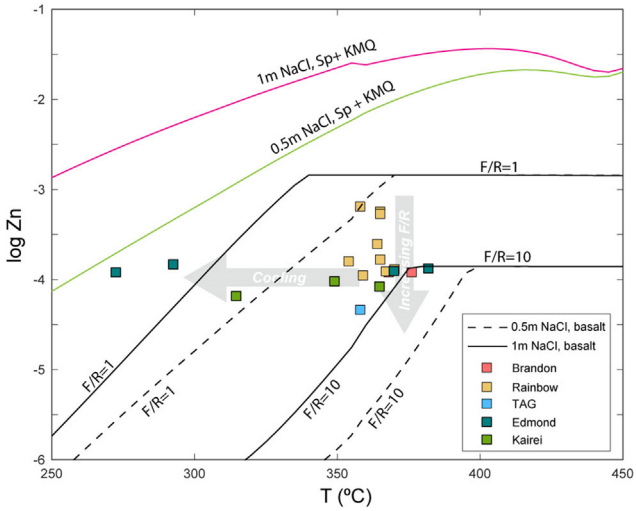

Fig. 10. Modeled Zn concentration as a function of temperature for fluids buffered by sphalerite + KMQ and by MORB. The green and pink lines show Zn concentration for fluids with 0.5 m and 1 m NaCl in sphalerite + KMQ buffered system. The black dashed lines and solid lines show Zn solubility in fluids with 0.5 m and 1 m NaCl in MORB buffered system. For MORB buffered system, the calculation was performed for fluid/rock ratio (F/R) of 1 and 10, respectively. Conductive cooling or changing fluid/rock ratio are potentially important factors affecting observed Zn solubility in vent fluids. Vent fluid data from Brandon (Von Damm et al., 2003), Rainbow (Seyfried et al., 2011), TAG (Edmonds et al., 1996), Edmond and Kairei (Gallant and Von Damm, 2006) hydrothermal systems were plotted in colored squares.

amounts of Zn can be hosted in silicates or iron oxides that make Zn less soluble compared to pure Zn minerals such as sphalerite or zincite. In effect, this is dictated by the lack of thermodynamic data and activity-concentration relations for compositionally more complex Zn-bearing minerals. However, the model reveals that fluid/rock ratio and/or the abundance and mineral specific distribution of Zn (i.e., silicates, iron oxides or sulfides) in the host rock can be important controls of the solubility of Zn in these and other seafloor hydrothermal systems, especially considering the fluids may form at deeper levels in the oceanic crust where temperature could be significantly higher than the venting temperature. It is also important to note that the observed metal solubility of vent fluids (e.g., Zn) may be affected by processes such as conductive cooling or by still further changes in fluid/rock ratio (Fig. 10). Thus, additional experimental and theoretical data for the composition and stability of Zn bearing minerals are needed if more quantitative models for Zn transport in subseafloor hydrothermal fluids are to be realized.

5. CONCLUSIONS

Hydrothermal experiments with chloride bearing aqueous fluids and sphalerite were performed to measure Zn solubility at 300–450 °C, 500 bar. The experiments took advantage of a newly designed Ti piston sampler that enables direct sampling at *in-situ* compositional conditions in a reliable and reproducible manner. The new Zn solubility data are consistent with values predicted using thermodynamic data from previous studies at 300–400 °C, but also reveal the considerable divergence between different thermodynamic datasets especially at temperatures above 400 °C. Such divergence can be resolved by adjusting the HKF EoS parameters of Zn^{2+} aqua ion based on the new experimental data and previous experimental and theoretical studies. Although empirical, this approach enables simulations of Zn transport within the popular HKF framework at fluid densities down to > 0.35 g/cm^3. Modelling the solubilities of Zn minerals (i.e., zincite, sphalerite) in Cl-bearing hydrothermal fluids with the new data shows good consistency with previous experiments at high T-P conditions. We show that temperature, fluid chlorinity and pH are important factors controlling Zn transport in hydrothermal fluids: in general, higher temperature, chlorinity and lower pH favor Zn transport. Speciation calculations show $ZnCl_3^-$ and $ZnCl_4^{2-}$ are the predominant species responsible for Zn transport in Cl-dominant acidic fluids at 250–450 °C. We further show that the observed Zn contents in vent fluids from seafloor hydrothermal systems are well undersaturated with sphalerite and more likely controlled by a combination of chemical and physical factors. Changes in fluid/rock mass ratio as well as the distribution and abundance of Zn in host minerals (other than sphalerite) play a key role in accounting for mass transfer reactions involving Zn. The new experimental data and the theoretical interpretation of Zn solubility in high T-P fluids allow better constrain of Zn transport in both subaerial and submarine hydrothermal systems.

Declaration of Competing Interest

The authors declare that they have no known competing financial interests or personal relationships that could have appeared to influence the work reported in this paper.

ACKNOWLEDGEMENTS

This research was supported by National Science Foundation (NSF) grant OCE # 1736679 to W.E.S. The authors thank

Amanda Tudor for helping with iodometric titration. We are grateful to George Dan Miron and two anonymous reviewers for helpful reviews that helped improve this manuscript, and to Associate Editor Zoltan Zajacz for handling this manuscript.

APPENDIX A. SUPPLEMENTARY DATA

Supplementary data to this article can be found online at https://doi.org/10.1016/j.gca.2022.03.026.

REFERENCES

Akinfiev N. N. and Tagirov B. R. (2014) Zn in hydrothermal systems: thermodynamic description of hydroxide, chloride, and hydrosulfide complexes. *Geochem. Int.* **52**, 197–214.

Alt-Epping P. and Smith L. (2001) Computing geochemical mass transfer and water/rock ratios in submarine hydrothermal systems: implications for estimating the vigour of convection. *Geofluids* **1**, 163–181.

Anderson A. J., Mayanovic R. and Bajt S. (1998) A microbeam XAFS study of aqueous chlrozinc complexing to 430°C in fluid inclusions from the Knaumühle granitic pegmatite, saxonian granulite massif, Germany. *Can. Mineral.* **36**, 511–524.

Barnes H. L. (1997) *Geochemistry of Hydrothermal Ore Deposits*. Wiley, New York.

Barrett T. J. and Anderson G. M. (1982) The solubility of sphalerite and galena in NaCl brines. *Econ. Geol.* **77**, 1923–1933.

Bau M. (1991) Rare-earth element mobility during hydrothermal and metamorphic fluid-rock interaction and the significance of the oxidation state of europium. *Chem. Geol.* **93**, 219–230.

Bethke C. M. (2007) *Geochemical and Biogeochemical Reaction Modeling*, 2nd ed. Cambridge University Press, Cambridge.

Bourcier W. L. and Barnes H. L. (1987) Ore solution chemistry. VII. Stabilities of chloride and bisulfide complexes of zinc to 350°C. *Econ. Geol.* **82**, 1839–1863.

Brugger J., Liu W., Etschmann B., Mei Y., Sherman D. M. and Testemale D. (2016) A review of the coordination chemistry of hydrothermal systems, or do coordination changes make ore deposits? *Chem. Geol.* **447**, 219–253.

Brugger J., Pring A., Reith F., Ryan C., Etschmann B., Liu W. H., O'Neill B. and Ngothai Y. (2010) Probing ore deposits formation: New insights and challenges from synchrotron and neutron studies. *Radiat. Phys. Chem.* **79**, 151–161.

Brugger J., McPhail D. C., Wallace M. and Waters J. (2003) Formation of Willemite in hydrothermal environments. *Econ. Geol.* **98**, 819–835.

Crerar D., Wood S., Brantley S. and Bocarsly A. (1985) Chemical controls on solubility of ore-forming minerals in hydrothermal solutions. *Can. Mineral.* **23**, 333–352.

Cygan G. L., Hemley J. J. and D'Angelo W. M. (1994) An experimental study of zinc chloride speciation from 300 to 600° C and 0.5 to 2kbar in buffered hydrothermal solutions. *Geochim. Cosmochim. Acta* **58**, 4841–4855.

de Ronde C. E. J., Massoth G. J., Butterfield D. A., Christenson B. W., Ishibashi J., Ditchburn R. G., Hannington M. D., Brathwaite R. L., Lupton J. E., Kamenetsky V. S., Graham I. J., Zellmer G. F., Dziak R. P., Embley R. W., Dekov V. M., Munnik F., Lahr J., Evans L. J. and Takai K. (2011) Submarine hydrothermal activity and gold-rich mineralization at Brothers Volcano, Kermadec Arc, New Zealand. *Miner. Depos.* **46**, 541–584.

Edmonds H. N., German C. R., Green D. R. H., Huh Y., Gamo T. and Edmond J. M. (1996) Continuation of the hydrothermal fluid chemistry time series at TAG, and the effects of ODP drilling. *Geophys. Res. Lett.* **23**, 3487–3489.

Etschmann B., Liu W., Mayanovic R., Mei Y., Heald S., Gordon R. and Brugger J. (2019) Zinc transport in hydrothermal fluids: on the roles of pressure and sulfur vs. chlorine complexing. *Am. Mineral.* **104**, 158–161.

Fernández D. P., Mulev Y., Goodwin A. R. H. and Sengers J. M. H. L. (1995) A database for the static dielectric constant of water and steam. *J. Phys. Chem. Ref. Data* **24**, 33–70.

Foustoukos D. I. and Seyfried W. E. (2005) Redox and pH constraints in the subseafloor root zone of the TAG hydrothermal system, 26° N Mid-Atlantic Ridge. *Earth Planet. Sci. Lett.* **235**, 497–510.

Fowler A. P. G., Scheuermann P., Tan C. and Seyfried W. (2019) Titanium reactors for redox-sensitive hydrothermal experiments: an assessment of dissolved salt on H2 activity-concentration relations. *Chem. Geol.* **515**, 87–93.

Gale A., Dalton C. A., Langmuir C. H., Su Y. and Schilling J.-G. (2013) The mean composition of ocean ridge basalts. *Geochemistry. Geophys. Geosyst.* **14**, 489–518.

Gallant R. M. and Von Damm K. L. (2006) Geochemical controls on hydrothermal fluids from the Kairei and Edmond Vent Fields, 23°–25°S, Central Indian Ridge. *Geochem., Geophys. Geosyst.* **7**, n/a–n/a.

Gamo T., Chiba H., Masuda H., Edmonds H. N., Fujioka K., Kodama Y., Nanba H. and Sano Y. (1996) Chemical characteristics of hydrothermal fluids from the TAG Mound of the Mid-Atlantic Ridge in August 1994: Implications for spatial and temporal variability of hydrothermal activity. *Geophys. Res. Lett.* **23**, 3483–3486.

German C. R. and Seyfried W. E. (2014) Hydrothermal processes. In *Treatise on Geochemistry*. Elsevier, Oxford, pp. 191–233.

Gysi A. P. and Harlov D. (2021) Hydrothermal solubility of $TbPO_4$, $HoPO_4$, $TmPO_4$, and $LuPO_4$ xenotime endmembers at pH of 2 and temperatures between 100 and 250 °C. *Chem. Geol.* **567** 120072.

Harris D. J., Brodholt J. P. and Sherman D. M. (2003) Zinc Complexation in Hydrothermal Chloride Brines: Results from *ab initio* Molecular Dynamics Calculations. *J. Phys. Chem. A* **107**, 1050–1054.

Helgeson H. C. (1969) Thermodynamics of hydrothermal systems at elevated temperatures and pressures. *Am. J. Sci.* **267**, 729–804.

Helgeson H. C., Kirkham D. H. and Flowers G. C. (1981) Theoretical prediction of the thermodynamic behavior of aqueous electrolytes by high pressures and temperatures; IV, Calculation of activity coefficients, osmotic coefficients, and apparent molal and standard and relative partial molal properties to 600 degrees C and 5kb. *Am. J. Sci.* **281**, 1249–1516.

Hemley J. J., Cygan G. L., Fein J. B., Robinson G. R. and d'Angelo W. M. (1992) Hydrothermal ore-forming processes in the light of studies in rock-buffered systems; I, Iron-copper-zinc-lead sulfide solubility relations. *Econ. Geol.* **87**, 1–22.

Ho P. C., Palmer D. A. and Gruszkiewicz M. S. (2001) Conductivity Measurements of Dilute Aqueous HCl Solutions to High Temperatures and Pressures Using a Flow-Through Cell. *J. Phys. Chem. B* **105**, 1260–1266.

Hurtig N. C. and Williams-Jones A. E. (2014) An experimental study of the solubility of MoO_3 in aqueous vapour and low to intermediate density supercritical fluids. *Geochim. Cosmochim. Acta* **136**, 169–193.

Ji F., Zhou H., Yang Q., Gao H., Wang H. and Lilley M. D. (2017) Geochemistry of hydrothermal vent fluids and its implications for subsurface processes at the active Longqi hydrothermal field, Southwest Indian Ridge. *Deep Sea Res. Part I Oceanogr. Res. Pap.* **122**, 41–47.

Liu W., Etschmann B., Foran G., Shelley M. and Brugger J. (2007) Deriving formation constants for aqueous metal complexes from XANES spectra: Zn^{2+} and Fe^{2+} chloride complexes in hypersaline solutions. *Am. Mineral.* **92**, 761–770.

Johnson J. W., Oelkers E. H. and Helgeson H. C. (1992) SUPCRT92: a software package for calculating the standard molal thermodynamic properties of minerals, gases, aqueous species, and reaction from 1 to 5000 bar and 0 to 1000 °C. *Comput. Geosci.* **18**(7), 899–947.

Liu W. H., Brugger J., Etschmann B., Testemale D. and Hazemann J. L. (2008) The solubility of nantokite (CuCl(s)) and Cu speciation in low-density fluids near the critical isochore: An in-situ XAS study. *Geochim. Cosmochim. Acta* **72**, 4094–4106.

Mayanovic R. A., Anderson A. J., Bassett W. A. and Chou I. (1999) XAFS measurements on zinc chloride aqueous solutions from ambient to supercritical conditions using the diamond anvil cell. *J. Synchrotron Radiat.* **6**, 195–197.

McDermott J. M., Sylva S. P., Ono S., German C. R. and Seewald J. S. (2018) Geochemistry of fluids from Earth's deepest ridge-crest hot-springs: Piccard hydrothermal field, Mid-Cayman Rise. *Geochim. Cosmochim. Acta* **228**, 95–118.

Meffre S., Large R. R., Steadman J. A., Gregory D. D., Stepanov A. S., Kamenetsky V. S., Ehrig K. and Scott R. J. (2016) Multi-stage enrichment processes for large gold-bearing ore deposits. *Ore Geol. Rev.* **76**, 268–279.

Mei Y., Liu W., Brugger J., Sherman D. M. and Gale J. D. (2018) The dissociation mechanism and thermodynamic properties of HCl(aq) in hydrothermal fluids (to 700 °C, 60 kbar) by ab initio molecular dynamics simulations. *Geochim. Cosmochim. Acta* **226**, 84–106.

Mei Y., Liu W., Sherman D. M. and Brugger J. (2014) Metal complexation and ion hydration in low density hydrothermal fluids: Ab initio molecular dynamics simulation of Cu(I) and Au(I) in chloride solutions (25–1000°C, 1–5000bar). *Geochim. Cosmochim. Acta* **131**, 196–212.

Mei Y., Sherman D. M., Liu W., Etschmann B., Testemale D. and Brugger J. (2015) Zinc complexation in chloride-rich hydrothermal fluids (25–600°C): A thermodynamic model derived from ab initio molecular dynamics. *Geochim. Cosmochim. Acta* **150**, 265–284.

Migdisov A. and Williams-Jones A. E. (2014) Hydrothermal transport and deposition of the rare earth elements by fluorine-bearing aqueous liquids. *Miner. Depos.* **49**, 987–997.

Migdisov A., Williams-Jones A. E. and Wagner T. (2009) An experimental study of the solubility and speciation of the Rare Earth Elements (III) in fluoride- and chloride-bearing aqueous solutions at temperatures up to 300°C. *Geochim. Cosmochim. Acta* **73**, 7087–7109.

Miron G. D., Leal A. M. M. and Yapparova A. (2019) Thermodynamic properties of aqueous species calculated using the HKF model: how do different thermodynamic and electrostatic models for solvent water affect calculated aqueous properties? ed Y. Mei. *Geofluids* **2019**, 5750390.

Mountain B. W. and Seward T. M. (2003) Hydrosulfide/sulfide complexes of copper(I): experimental confirmation of the stoichiometry and stability of $Cu(HS)_2^-$ to elevated temperatures. *Geochim. Cosmochim. Acta* **67**, 3005–3014.

Murcia D. C. F., Fosbøl P. L., Thomsen K. and Stenby E. H. (2017) Determination of zinc sulfide solubility to high temperatures. *J. Solution Chem.* **46**, 1805–1817.

Neff J. M. (2002) Zinc in the ocean. In *Bioaccumulation in Marine Organisms*. Elsevier, Oxford, pp. 175–189.

Oelkers E. H. and Helgeson H. C. (1990) Triple-ion anions and polynuclear complexing in supercritical electrolyte solutions. *Geochim. Cosmochim. Acta* **54**, 727–738.

Oelkers E. H. and Helgeson H. C. (1991) Calculation of activity coefficients and degrees of formation of neutral ion pairs in supercritical electrolyte solutions. *Geochim. Cosmochim. Acta* **55**, 1235–1251.

Plyasunov A. V. and Ivanov I. P. (1990) The solubility of zinc oxide in sodium chloride solutions up to 600°C and 1000 bar. *Geokhimiya* **11**, 1605–1617.

Pokrovski G. S., Roux J. and Harrichoury J.-C. (2005) Fluid density control on vapor-liquid partitioning of metals in hydrothermal systems. *Geology* **33**, 657–660.

Rempel K. U., Liebscher A., Meixner A., Romer R. L. and Heinrich W. (2012) An experimental study of the elemental and isotopic fractionation of copper between aqueous vapour and liquid to 450°C and 400bar in the CuCl–NaCl–H_2O and CuCl–NaHS–NaCl–H_2O systems. *Geochim. Cosmochim. Acta* **94**, 199–216.

Rietveld H. M. (1969) A profile refinement method for nuclear and magnetic sturctures. *J. Appl. Crystallogr.* **2**, 65–71.

Ruaya J. R. and Seward T. M. (1986) The stability of chlorozinc (II) complexes in hydrothermal solutions up to 350°C. *Geochim. Cosmochim. Acta* **50**, 651–661.

Scheuermann P. P., Syverson D. D., Higgins J. A., Pester N. J. and Seyfried W. E. (2018a) Calcium isotope systematics at hydrothermal conditions: mid-ocean ridge vent fluids and experiments in the $CaSO_4$-NaCl-H_2O system. *Geochim. Cosmochim. Acta* **226**, 18–35.

Scheuermann P. P., Tan C. and Seyfried W. E. (2018b) Quartz solubility in the two-phase region of the NaCl-H_2O system: an experimental study with application to the piccard hydrothermal field, mid-cayman rise. *Geochem. Geophys. Geosystems* **19**, 3570–3582.

Scheuermann P. P., Tutolo B. M. and Seyfried W. E. (2019) Anhydrite solubility in low-density hydrothermal fluids: experimental measurements and thermodynamic calculations. *Chem. Geol.* **524**, 184–195.

Scheuermann P. P., Xing Y., Ding K. and Seyfried W. E. (2020) Experimental measurement of H_2(aq) solubility in hydrothermal fluids: application to the Piccard hydrothermal field, Mid-Cayman Rise. *Geochim. Cosmochim. Acta* **283**, 22–39.

Schmidt C., Watenphul A., Jahn S., Schäpan I., Scholten L., Newville M. G. and Lanzirotti A. (2018) Copper complexation and solubility in high-temperature hydrothermal fluids: a combined study by Raman, X-ray fluorescence, and X-ray absorption spectroscopies and ab initio molecular dynamics simulations. *Chem. Geol.* **494**, 69–79.

Seward T. M. (1976) The stability of chloride complexes of Silver in hydrothermal solutions up to 350°C. *Geochim. Cosmochim. Acta* **40**, 1329–1341.

Seward T. M. and Barnes H. L. (1997) Chapter 9: metal transport by hydrothermal ore fluids. In *Geochemistry of Hydrothermal Ore Deposits*. John Willey & Sons, pp. 435–486.

Seyfried W. E., Gordon P. C. and Dickson F. W. (1979) A new reaction cell for hydrothermal solution equipment. *Am. Mineral.* **64**, 646–649.

Seyfried W. E. and Ding K. (1995) Phase equilibria in subseafloor hydrothermal systems: a review of the role of redox, temperature, Ph and dissolved Cl on the chemistry of hot spring fluids at mid-ocean ridges. In *Seafloor Hydrothermal Systems: Physical, Chemical, Biological, and Geological Interactions*. American Geophysical Union, pp. 248–272.

Seyfried W. E., Janecky D. R. and Berndt M. E. (1987) Rocking autoclaves for hydrothermal experiments II: the flexible cell system. In *Experimental Hydrothermal Techniques* (eds. G. Ulmer and H. L. Barnes). Wiley Interscience, pp. 216–240.

Seyfried Jr. W. E., Pester N. J., Ding K. and Rough M. (2011). *Geochim. Cosmochim. Acta* **75**, 1574–1593.

Please cite this article in press as: Xing Y., et al. An experimental and thermodynamic study of sphalerite solubility in chloride-bearing fluids at 300–450 °C, 500 bar: implications for zinc transport in seafloor hydrothermal systems. *Geochim. Cosmochim. Acta* (2022), https://doi.org/10.1016/j.gca.2022.03.026

Seyfried W. E. and Mottl M. J. (1982) Hydrothermal alteration of basalt by seawater under seawater-dominated conditions. *Geochim. Cosmochim. Acta* **46**, 985–1002.

Seyfried W. E., Seewald J. S., Berndt M. E., Ding K. and Foustoukos D. I. (2003) Chemistry of hydrothermal vent fluids from the Main Endeavour Field, northern Juan de Fuca Ridge: Geochemical controls in the aftermath of June 1999 seismic events. *J. Geophys. Res. Solid Earth*, 108.

Shmulovich K. I., Heinrich W., Möller P. and Dulski P. (2002) Experimental determination of REE fractionation between liquid and vapour in the systems NaCl-H_2O and $CaCl_2$-H_2O up to 450°C. *Contrib. Mineral. Petrol.* **144**, 257–273.

Shock E. L. and Helgeson H. C. (1988) Calculation of the thermodynamic and transport properties of aqueous species at high pressures and temperatures: correlation algorithms for ionic species and equation of state predictions to 5kb and 1000° C. *Geochim. Cosmochim. Acta* **52**, 2009–2036.

Shock E. L., Sassani D., Willis M. and Sverjensky D. A. (1997) Inorganic species in geologic fluids: correlations among standard molal thermodynamic properties of aqueous ions and hydroxide complexes. *Geochim. Cosmochim. Acta* **61**, 907–950.

Shvarov Y. (1999) Algorithmization of the numeric equilibrium modeling of dynamic geochemical processes. *Geochem. Int.* **37**, 571–576.

Shvarov Y. (2015) A suite of programs, OptimA, OptimB, OptimC, and OptimS compatible with the Unitherm database, for deriving the thermodynamic properties of aqueous species from solubility, potentiometry and spectroscopy measurements. *Appl. Geochem.* **55**, 17–27.

Shvarov Y. and Bastrakov E. (1999) *HCh: a software package for geochemical equilibrium modelling*. User's Guide.

Stefánsson A. and Seward T. M. (2004) Gold(I) complexing in aqueous sulphide solutions to 500°C at 500 bar. *Geochim. Cosmochim. Acta* **68**, 4121–4143.

Susak N. J. and Crerar D. A. (1985) Spectra and coordination changes of transition metals in hydrothermal solutions: implications for ore genesis. *Geochim. Cosmochim. Acta* **49**, 555–564.

Sverjensky D. A., Shock E. L. and Helgeson H. C. (1997) Prediction of the thermodynamic properties of aqueous metal complexes to 1000°C and 5 kb. *Geochim. Cosmochim. Acta* **6**, 1359–1412.

Syverson D. D., Scheuermann P., Higgins J. A., Pester N. J. and Seyfried W. E. (2018) Experimental partitioning of Ca isotopes and Sr into anhydrite: Consequences for the cycling of Ca and Sr in subseafloor mid-ocean ridge hydrothermal systems. *Geochim. Cosmochim. Acta* **236**, 160–178.

Tagirov B. R. and Seward T. M. (2010) Hydrosulfide/sulfide complexes of zinc to 250°C and the thermodynamic properties of sphalerite. *Chem. Geol.* **269**, 301–311.

Tagirov B. R., Suleimenov O. M. and Seward T. M. (2007) Zinc complexation in aqueous sulfide solutions: Determination of the stoichiometry and stability of complexes via ZnS(cr) solubility measurements at 100°C and 150bars. *Geochim. Cosmochim. Acta* **71**, 4942–4953.

Tagirov B. R., Trigub A. L., Filimonova O. N., Kvashnina K. O., Nickolsky M. S., Lafuerza S. and Chareev D. A. (2019) Gold transport in hydrothermal chloride-bearing fluids: insights from in situ X-ray absorption spectroscopy and ab initio molecular dynamics. *ACS Earth Sp. Chem.* **3**, 240–261.

Tagirov B. R., Zotov A. V. and Akinfiev N. N. (1997) Experimental study of dissociation of HCl from 350 to 500°C and from 500 to 2500 bars: thermodynamic properties of HCl°(aq). *Geochim. Cosmochim. Acta* **61**, 4267–4280.

Thébaud N., Philippot P., Rey P., Brugger J., Van Kranendonk M. and Grassineau N. (2008) Protracted fluid–rock interaction in the Mesoarchaean and implication for gold mineralization: example from the Warrawoona syncline (Pilbara, Western Australia). *Earth Planet. Sci. Lett.* **272**, 639–655.

Tivey M. K. (1995) The influence of hydrothermal fluid composition and advection rates on black smoker chimney mineralogy: insights from modeling transport and reaction. *Geochim. Cosmochim. Acta* **59**, 1933–1949.

Von Damm K. L., Lilley M. D., Shanks III W. C., Brockington M., Bray A. M., O'Grady K. M., Olson E., Graham A., Proskurowski G. and the SouEPR Science Party (2003). *Earth Planet. Sci. Lett.* **206**(3–4), 365–378.

Xing Y., Brugger J., Tomkins A. and Shvarov Y. (2019a) Arsenic evolution as a tool for understanding formation of pyritic gold ores. *Geology* **47**, 335–338.

Xing Y., Mei Y., Etschmann B., Liu W. and Brugger J. (2018) Uranium transport in F-Cl-bearing fluids and hydrothermal upgrading of U-Cu ores in IOCG deposits. *Geofluids* **2018**, 1–22.

Xing Y., Etschmann B., Liu W., Mei Y., Shvarov Y., Testemale D., Tomkins A. and Brugger J. (2019b) The role of fluorine in hydrothermal mobilization and transportation of Fe, U and REE and the formation of IOCG deposits. *Chem. Geol.* **504**, 158–176.

Xing Y., Scheuermann P. and Seyfried W. E. (2021) Experimental study on Fe solubility in vapor-rich hydrothermal fluids at 400–500 °C, 215–510 bar: implication for Fe mobility in seafloor vent systems. *Geochim. Cosmochim. Acta* **314**, 209–222.

Yardley B. (2005) Metal concentrations in crustal fluids and their relationship to ore formation. *Econ. Geol.* **100**, 613–632.

Zhong R., Brugger J., Chen Y. and Li W. (2015) Contrasting regimes of Cu, Zn and Pb transport in ore-forming hydrothermal fluids. *Chem. Geol.* **395**, 154–164.

Associate editor: Zoltan Zajacz

Please cite this article in press as: Xing Y., et al. An experimental and thermodynamic study of sphalerite solubility in chloride-bearing fluids at 300–450 °C, 500 bar: implications for zinc transport in seafloor hydrothermal systems. *Geochim. Cosmochim. Acta* (2022), https://doi.org/10.1016/j.gca.2022.03.026